Petroleum Science 20 (2023) 3673–3686

Contents lists available at ScienceDirect

Petroleum Science

journal homepage: www.keaipublishing.com/en/journals/petroleum-science

Original Paper

Cuttings transport: Back reaming analysis based on a coupled layering-sliding mesh method via CFD

Na Zhu [a, *], Shi-Dong Ding [b], Xiao-Lei Shi [a], Wen-Jun Huang [a, **], De-Li Gao [a, ***]

[a] MOE Key Laboratory of Petroleum Engineering, China University of Petroleum, Beijing, 102249, China
[b] SINOPEC Research Institute of Petroleum Engineering Co. Ltd, No. 197 Baisha Road, Changping District, Beijing, 102206, China

ARTICLE INFO

Article history:
Received 23 August 2022
Received in revised form
23 February 2023
Accepted 25 June 2023
Available online 4 July 2023

Edited by Jia-Jia Fei

Keywords:
Drill cuttings transport
Back reaming
Layering-sliding mesh
Hole cleaning
Connector

ABSTRACT

Inadequate hole cleaning is one of the main reasons for inefficient operations in extended-reach drilling. The mechanism of cuttings transport under the back reaming operation, which is frequently adopted to remove the cuttings, has been investigated in this study. To this end, a coupled layering-sliding mesh method with the Eulerian-Granular approach has been established innovatively. The dynamic layering method has been employed to simulate the axial motion of the pipe, whereas the sliding mesh method has been used to simulate the pipe rotation. The back reaming operation of a connector-furnished pipe has been simulated, and the sensitive parameter analysis has been conducted. The results thus obtained demonstrate that the increase in the initial bed height, inclination, and the diameter and length of the connector causes a significant increase in the cuttings concentration. In addition, the cuttings concentration is observed to decrease significantly with the pipe rotation speed. Furthermore, two main factors contribute towards the cuttings accumulation around the connector, namely, the difference in the cross-sectional area and the pushing effect of the connector—like a "bulldozer". The "bulldozer" effect of the connector dominates when the tripping velocity is significant compared to the velocity of the cuttings. Conversely, the effect of the difference in the cross-sectional area becomes the leading factor for cuttings accumulation. The "bulldozer" effect of the connector causes a more severe impact on hole cleaning. In both cases, increasing the tripping velocity only mildly affects the cuttings concentration. It is therefore suggested that the tripping velocity should be slower than that of the sand during the back reaming operation. Furthermore, increased fluid velocity might lead to a higher accumulated cuttings concentration around the connector when the cuttings bed has not entirely passed through the connector. A significant flow rate can be safely applied after the cuttings have passed through the connector furnished with a large diameter, such as the bottom hole assembly. This exploration serves as an essential guide to predicting and controlling tight spots while back reaming.

1. Introduction

A drilling project is fundamentally reliant on hole cleaning, which is an essential component contributing to the overall efficiency and profitability of a drilling project (Alshaikh et al., 2018). Given the comprehensive impact of hole cleaning, inadequate execution thereof may result in a wide array of problems, such as increased equivalent circulating density and formation leakage, low ROP, high drag or torque of the pipe string, or even stuck pipe accidents (Epelle and Gerogiorgis, 2019). Given the scope of issues that may occur, it is essential to note that a high proportion of stuck pipe events, estimated at around 54%, occur during the execution of tripping and back reaming (Yarim et al., 2007).

Back reaming is an operation that combines pumping, pipe rotating, and pulling out of the hole (Paranhos Sobrinho et al., 2021; Yarim et al., 2010). This operation has gained popularity due to its ability to solve poor hole conditions while tripping. However, it is also infamous for being risky on extended-reach wells (Yarim et al., 2007). This operation cleans the wellbore entirely below the bottom hole assembly (BHA) rather than leaving a small cuttings bed.

* Corresponding author.
** Corresponding author.
*** Corresponding author.
E-mail addresses: 931819658@qq.com (N. Zhu), huangwenjun@cup.edu.cn (W.-J. Huang), gaodeli_team@126.com (D.-L. Gao).

https://doi.org/10.1016/j.petsci.2023.06.009

As such, a dangerous cuttings dune is built up just above the BHA, thereby significantly increasing the risk of packing off and stuck pipe (Zhu et al., 2022).

Two primary procedures are involved in hole cleaning, namely drilling and washing. However, the investigation on cuttings transport under back reaming conditions is also important, although current research regarding the effects is largely insufficient. To this end, the investigation of cuttings transport is mainly considered to be experimental and theoretical research.

The influence of several variables on hole cleaning can be studied experimentally (Pandya et al., 2019; Song et al., 2017; Ozbayoglu et al., 2008). It can be determined that the current shortcomings of this line of inquiry (Pang et al., 2019) arise from the variations in wellbore geometry, solid characteristics, flow parameters, etc., resulting in complications of testing execution under a majority of flow conditions. Specifically, when considering the impact of drilling and washing, these components are generally observed through the combination of the flow and drilling rate. However, the pipe is often assumed to be stationary or merely rotating. Specific experiments investigating back reaming, as well as a coupling of axial and rotational pipe movement, are complex, more difficult, and scarcely conducted.

Layer-modeling and computational fluid dynamics (CFD) are the two main primary theoretical approaches used to investigate hole cleaning. Layer-modeling facilitates effective simulation of the cuttings transport along the entire wellbore with a fast-computing speed. However, most layer models are still based exclusively on the two procedures of washing & drilling (Li and Luft, 2014a; Cho et al., 2002; Nguyen and Rahman, 1998; Gavignet and Sobey, 1989). Given that the drill pipe rotation mechanism is rather complicated (Guo et al., 2010), models of back reaming featuring a coupling of axial and rotational pipe motion have yet to be perfectly simulated (Zhu et al., 2022).

The CFD method, which aims to determine how cuttings are transported in the annular wellbore, is popular among researchers and readily employed (Zhang et al., 2020; Heydari et al., 2017). This method exhibits the advantage of providing detailed accounts pertaining to the desired properties without limiting experimental conditions or layer models (Bicalho et al., 2016). Variables such as fluid velocity and rheological properties, ROP, the drill pipe rotational effect, etc., have all been extensively investigated using the CFD method. However, even when considering the efficacy and popularity of this approach, no model exists that can accurately forecast cuttings' concentration during back reaming. This lack of investigative methodology is solely attributed to the computational bottleneck created by the immense flow complexity caused by the coupled motion of the pipe.

CFD simulations can be conducted using two types of methods: Eulerian-Eulerian and Eulerian-Lagrangian (Table 1 in Appendix A). The former treats both the fluid phase and the particles as continuum phases. This approach can effectively represent many particles at little computational expense, although it is unable to provide comprehensive details regarding the flow at the micro- and mesoscales (Zhang et al., 2018). Then, using the Eulerian-Lagrangian approach, particles are treated as discrete phases, making it possible to determine the motion of each particle separately and thereby better analyze the particle collisions (Akhshik et al., 2015; Capecelatro and Desjardins, 2013). Although providing improved individual particulate analyses, the disadvantage of the Eulerian-Lagrangian approach is that its computational cost is much higher than that of the former Eulerian-Eulerian approach, especially when considering flows containing many particles. Additionally, it is difficult to converge when combined with moving mesh. As a variant of the Eulerian-Eulerian approach, the Eulerian-Granular model enables the modeling of multiple, separate, and interacting phases. This method treats the solid phase as a continuous 'fluid' phase via the Eulerian approach and is only differentiated by designating it as a granular phase, which can input the granular parameters, such as diameter and packing limit. This method requires fewer computational resources and is used extensively in studying liquid-solid flows (Basu et al., 2015; Bonamy et al., 2009).

To this end, a novel coupled layering-sliding mesh method with the Eulerian-Granular approach has been proposed in this study to investigate the back reaming operation. In this method, the dynamic layering method is employed to simulate the axial motion of the pipe, whereas the sliding mesh model simulates the pipe rotation action. This article intends to provide some perspectives on the mechanism of the cuttings transport under the back reaming operation and propose an optimization strategy to lessen and control the pipe sticking risks.

2. Mechanism of back reaming

Back reaming is defined as a mechanical operation combing pumping, pipe rotating, and extraction from the hole (Fig. 1). This method is widely adopted when there is a problem with tripping out of the hole (Yarim et al., 2010). However, its use on extended reach wells has garnered a notorious negative connotation for being high risk. Furthermore, the supposed advantages of back reaming for cuttings transport might in fact have an overall negative influence on hole cleaning. To investigate the mechanisms entailed in back reaming, four aspects of the process will be accordingly analyzed as follows :

2.1. Impact of the circulation

Liquid phase circulation generates a shear force at the interface to efficiently erode the cuttings bed and is vital for cutting removal (Li and Luft, 2014b). Most studies have demonstrated that fluid circulation positively affects cutting transport (Mahmoud et al., 2020).

Nonetheless, it is important to note that the incidence of higher circulation during cutting removal can also subsequently increase the risk of pipe sticking, mainly because the fluid velocity increases when there is a connector with a greater diameter and smaller cross-sectional area than the pipe body. The fluid velocity behind

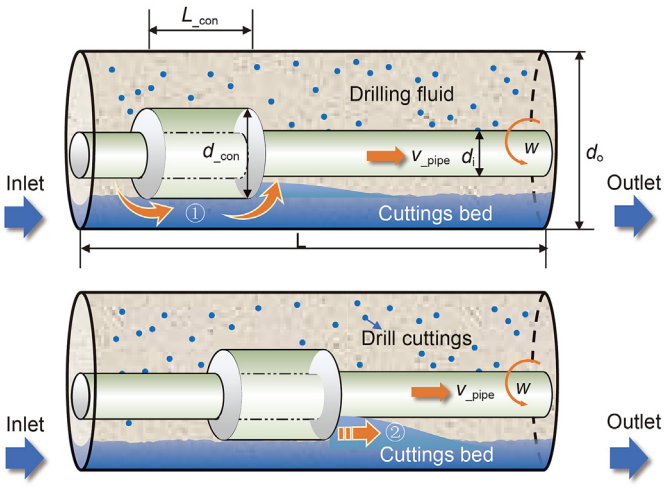

Fig. 1. Schematic illustration of the back reaming operation with a connector (①Sudden change of flow velocity leading to cuttings accumulation; ②Push effect of the connector on cuttings like a"bulldozer").

the connector then reduces, resulting in an accumulation of cuttings as they stack up into a pile. Thus, the key to enabling complete and full use of the circulation is investigating how it influences the cuttings concentration with the existing connectors and then manipulating it within the predetermined safe value.

2.2. The axial motion of the pipe

The pipe moves upwards to the wellhead while back reaming, exerting a shear force on cuttings. Whether the shear force is regarded as propulsion or resistance, force is determined by the relative speed of the drill pipe and cuttings. More specifically, when the tripping velocity exceeds that of the velocity of the cuttings, the cuttings' shear force from the pipe acts as a propulsion force; otherwise, it acts as a resistance force.

When considering these aspects, one can regard the fact that the presence of a propulsion force does not necessarily entail a benefit for hole cleaning. When there is a connector present, the propulsion force from the pipe connector may push the cuttings bed like a "bulldozer" thus causing the cuttings to pile up behind the connector. The layering method is employed to simulate the axial motion of the pipe (Section 3.3.1).

2.3. The rotational motion of the pipe

Pipe rotation positively affects cuttings' removal since the tangential velocity of the pipe can directly affect the axial velocity of the cuttings' phase. Furthermore, the extra drag disperses and lifts the settled cuttings into the broader areas (Cayeux et al., 2014; Heydari et al., 2017). The sliding mesh model simulates the pipe rotation (Section 3.3.2).

2.4. Impact of the connectors

The connectors' diameter is larger than that of the pipe body, which may represent tool joints, stabilizers, BHA components (Yarim et al., 2010), etc. When considering the presence of a connector, the propulsion force acting upon the cuttings, either from the circulation or the tripping pipe, may change from a positive to a negative influence when observed in the context of hole cleaning. For example, circulation is recognized as a beneficial factor for cuttings removal. However, the difference in the cross-sectional area around the connectors and the corresponding change in the fluid velocity may cause cuttings to accumulate behind the connectors. These accumulated cuttings may result in a pile that can in turn lead to a stuck pipe while tripping. In this specific case, the presence of the connector may result in circulation being considered disadvantageous. Therefore, the total effect of the connectors on back reaming requires further investigation to portray a more functional, positive comprehension thereof.

3. Methodology

3.1. CFD model description

As a variant of the Eulerian-Eulerian approach, the Eulerian-Granular method considers the particle phase as a separate continuous phase, and two-phase interpenetrating continua represent the fluid-particle mixture (Basu et al., 2015). This method requires less computational resources and has been extensively used in liquid-solid flows. The detailed equations are presented in section 3.2.

The computational domain comprises a horizontal annulus with a borehole as well as a pipe that rotates eccentrically, and has a connector. In Fig. 2, the horizontal annulus' computational grid is displayed. The parameters of the geometry and the simulation setup parameters are all shown in Table 1.

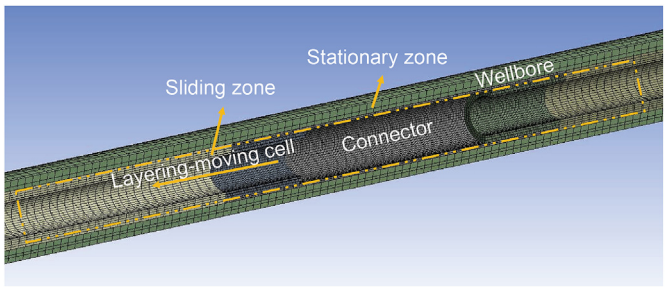

Fig. 2. Annular flow geometry with a connector.

3.2. Mathematical formulation

3.2.1. Mass conservation

The mass conservation is given by (Fluent, 2021):

$$\frac{\partial}{\partial t}(\alpha_q \rho_q) + \nabla \cdot \left(\alpha_q \rho_q \vec{v}_q\right) = \sum_{s=1}^{n}(\dot{m}_{sq} - \dot{m}_{qs}) \tag{1}$$

where, $\vec{v}_q$ is the velocity, $\dot{m}$ is the mass transfer of the two phases, α is the volume fraction of each phase, ρ is density, q and s represent the liquid and solid phases, separately.

3.2.2. Conservation of momentum

The momentum conservation for the phase q is:

$$\begin{aligned}\frac{\partial}{\partial t}\left(\alpha_q \rho_q \vec{v}_q\right) + \nabla \cdot \left(\alpha_q \rho_q \vec{v}_q \vec{v}_q\right) &= -\alpha_q \nabla p + \nabla \cdot \bar{\bar{\tau}}_q + \alpha_q \rho_q \vec{g} \\ &+ \sum_{s=1}^{n}\left(\vec{R}_{sq} + \dot{m}_{sq}\vec{v}_{sq} - \dot{m}_{qs}\vec{v}_{qs}\right) \\ &+ \left(\vec{F}_q + \vec{F}_{lift,q} + \vec{F}_{wl,q} + \vec{F}_{vm,q} + \vec{F}_{td,q}\right)\end{aligned} \tag{2}$$

where, $\vec{F}_q$ and $\vec{F}_{vm,q}$ is the external body force and virtual mass force, $\bar{\bar{\tau}}_q$ is the stress-strain tensor for the q^{th} phase, $\vec{F}_{lift,q}$ and $\vec{F}_{td,q}$ is the lift force and turbulent dispersion force, $\vec{F}_{wl,q}$ is a lubrication force of the wall, $\vec{R}_{sq}$ is the force between two phases, $\vec{v}_{sq}$ is the relative velocity, and p is pressure.

3.2.3. Granular temperature

For the solids phase, the granular temperature is expressed by:

$$\Theta_s = \frac{1}{3}u_s u_s \tag{3}$$

where, u_s is the fluctuating solids velocity.

The transport equation based on kinetic theory is given by:

$$\begin{aligned}\frac{3}{2}\left[\frac{\partial}{\partial t}(\rho_s \alpha_s \Theta_s) + \nabla \cdot \left(\rho_s \alpha_s \vec{v}_s \Theta_s\right)\right] &= (-p_s \bar{\bar{I}} + \bar{\bar{\tau}}_s) \\ &: \nabla \cdot \vec{v}_s + \nabla \cdot (k_{\Theta_s} \nabla \Theta_s) - \gamma_{\Theta_s} + \varphi_{ls}\end{aligned} \tag{4}$$

where, $(-p_s \bar{\bar{I}} + \bar{\bar{\tau}}_s) : \nabla \cdot \vec{v}_s$ is the energy generated due to the stress tensor, $k_{\Theta_s}\nabla\Theta_s$ is the energy diffusion, γ_{Θ_s} is the energy dissipation due to collision, φ_{ls} is the energy transfer of two phases.

3.2.4. Solids pressure

The solids pressure is expressed by:

$$p_s = \alpha_s \rho_s \Theta_s + 2\rho_s(1+e_{ss})\alpha_s^2 g_{0,ss}\Theta_s \quad (5)$$

where, e_{ss} is the restitution coefficient, $g_{0,ss}$ is the radial distribution function.

3.2.5. Solids shear stresses

The solids stress tensor includes three components of viscosities:

$$\mu_s = \mu_{s,\mathrm{col}} + \mu_{s,\mathrm{kin}} + \mu_{s,\mathrm{fr}} \quad (6)$$

where, $\mu_{s,\mathrm{col}}$, $\mu_{s,\mathrm{kin}}$ and $\mu_{s,\mathrm{fr}}$, represents the collisional section, kinetic section, and frictional section of the viscosity.

3.3. Meshing scheme for the coupled motion of translation and rotation of the pipe

For the back reaming process, the drill pipe moves out via a coupled translation and rotation motion, and the sliding mesh and layering are employed simultaneously to simulate the above procedure.

3.3.1. Dynamic layering mesh method

In deforming regions subject to the boundary motion, three approaches are available for updating the volume mesh: smoothing, dynamic layering, as well as local remeshing. The dynamic layering method can increase or decrease layers of cells next to a moving boundary, and can simulate the translation movement of the pipe while tripping. The cells of layer j are merged or split with cells of the next layer i depending on the cells height of layer j (Fig. 3).

The cell heights of the layer j may increase till:

$$h_{\min} > (1+\alpha_s)h_{\mathrm{ideal}} \quad (7)$$

where, $h_{\min}$ and h_{ideal} is the minimum and the ideal height of the cell, and α_s is the split coefficient. The cells are divided following the specified height or ratio when the condition in Eq. (7) is satisfied.

Table 1
List of input data for modeling.

Variables	Symbols	Values	Units
Flow Geometry			
Wellbore diameter	d_o	73.9	mm
Pipe outer diameter	d_i	33.3	mm
Connector diameter	$d_{\_con}$	46.0	mm
Length of pipe	L	3	m
Length of connector	$L_{\_con}$	0.25	m
Fluid Properties			
Drilling fluid density	ρ_f	998.5	kg/m^3
Consistency coefficient	K	0.001	Pa·s^n
Flow behaviour index	n	1.0	dimensionless
Particle Properties			
Cuttings density	ρ_c	2500	kg/m^3
Cuttings diameter	d_p	3.0	mm
Drilling variables			
Pipe rotation speed	w	120	RPM
Tripping velocity	$v_{\_pipe}$	0.1	m/s
Eccentricity	e	0.3	dimensionless
Inclination	θ	90	°
Initial and boundary conditions			
Inlet velocity of water	$v_{\_water}$	1	m/s
Inlet velocity of sand	$v_{\_sand}$	0	m/s
Temperature	T	298	K
Pressure	P	0	psig

The cell heights of the layer j may decrease till:

$$h_{\min} < \alpha_c h_{\mathrm{ideal}} \quad (8)$$

where, α_c is the layer collapse factor. Cells in the compressed layer are merged with the above layer when the condition Eq. (8) is met; that is, layer j is merged into the layer i.

3.3.2. Sliding mesh method

The sliding mesh method can adequately define the entire transient startup, which is the most accurate method to simulate rotating flows (Fluent, 2021). This technique has two separate cell zones. One of the cell zones is attached to the drill pipe (rotating region), while the other is attached to the annulus between the pipe and casing (stationary region). Sliding-mesh interfaces are formed between rotating and stationary zones. Those interfaces can be arbitrary mesh interfaces (AMI), which can patch the geometries of both cell zones (Ramírez et al., 2015). Despite being geometrically separated, the two subdomains are numerically connected by AMI, which ensures that generic fields on all surfaces have the same value (Fluent, 2021). Thus, communication between the stationary and the rotating meshes is realized through interfaces (Zhang and Liang, 2015).

A closer look at Fig. 4 reveals how stationary and rotating regions on the sliding-mesh interface are connected. The sliding region covers the drill pipe as well as the connector, and the stationary zone is from the interface to the wellbore. On the other hand, both the drill pipe and the connector move along the axial wellbore, thus achieving the combined motion of translation and rotation of the pipe.

3.4. Simulation strategy

The Reynolds Averaged Navier Stokes (RANS) equations (continuity and momentum equations) are numerically solved in a discretized domain using the finite-volume formulation. The coupled Semi-Implicit Method for Pressure-Linked Equations (SIMPLE) scheme is applied for the solution. The effect of numerical diffusion on the solution accuracy is mitigated by employing second-order accurate solution schemes (Second Order Upwind) for the momentum and turbulent parameters. The volume fraction is spatially discretized using the Quadratic Upstream Interpolation for Convective Kinematics (QUICK) method. Also, under-relaxation factors were appropriately tuned to ensure stable convergence. A velocity inlet boundary condition (Table 1) is specified alongside a pressure outlet at atmospheric pressure. The wall boundaries were treated according to the conventional fluid mechanic's no-slip condition. Furthermore, a constant time step of 1×10^{-4} s for satisfactory convergence is used in all simulations. The simulation procedure for the Eulerian–Granular model via Ansys Fluent is presented in Fig. 5.

3.5. CFD model validation

As mentioned earlier, both the experiment and simulation on the coupled motion of translation and rotation of pipe, i.e., the tripping process, are very scarce, so there is little data that can be used to verify the coupled translation and rotation motion. However, the employed Eulerian-Granular method can be verified by the drilling process. In Fig. 6(a), Garcia-Hernandez et al. (2007) provide some experimental measurements of moving bed velocity with a cutting diameter of 4 mm and the ROP of 30 ft/h. The mean absolute percentage error of the prediction is 5.7%. Similar predictions have been conducted by Duan et al. (2008) via experiments in which the cutting diameter is 1.4 mm, and the ROP is

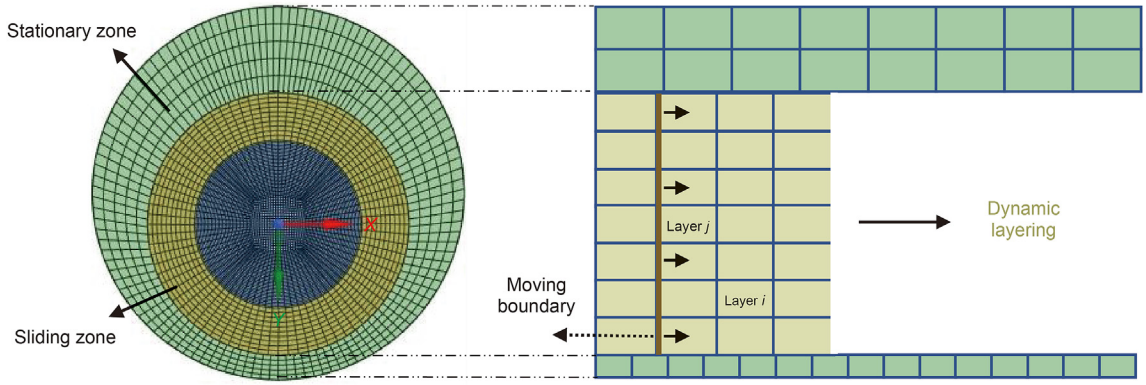

Fig. 3. Schematic illustration of the dynamic layering.

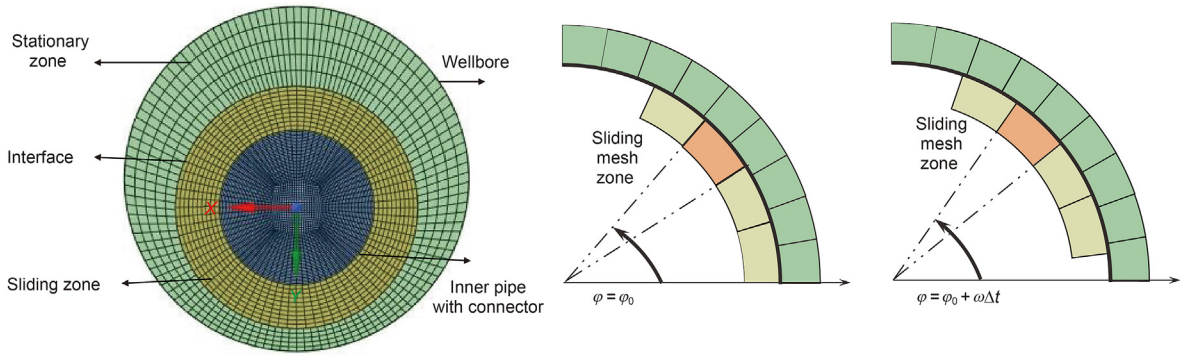

Fig. 4. Schematic illustration of the sliding mesh concept.

30 ft/h. The Eulerian-Granular model yields a mean error of less than 10% (Fig. 6(b)). The cuttings concentration at a higher flow rate is difficult to predict (the error is 13%); this is because the particle-fluid interaction is complex considering the turbulence, and the inhomogeneity of particle size is not considered. Besides, Fig. 6(c) and (d) present the mean errors of less than 10% via the Eulerian-Granular models in addition. Overall, Fig. 6 shows that the model matches well with the experimental data (Duan et al., 2008; Garcia-Hernandez et al., 2007; Osgouei, 2010; Han et al., 2010); thus, the capability of the Eulerian-Granular model can reasonably predict the cuttings concentration.

4. Results and discussion

4.1. Impact of the circulation time

An initial cuttings bed with a height of 10% of wellbore diameter (d_o) with a packed porosity of 52% is distributed along the annulus (average cuttings concentration is 6%). The contours of cuttings concentration under different circulation time while back reaming are presented in Fig. 7. As observed in Fig. 7(a), the pipe and cuttings bed move towards the outlet with time. However, it also can be found that cuttings pile up behind the connector, which has a risk of getting pipes stuck. The reason may be that the velocity of water decreases behind the connector as a result of the increase of the cross-sectional area (Fig. 7(b)), resulting in an accumulation of cuttings as they stack up into a pile.

The impact of the circulation time on the cuttings concentration of the cross-section is presented in Fig. 8. The cuttings are transported via water, and pile up behind the connector, resulting in a higher concentration and higher risk behind the connector. The highest concentration can achieve 12.8%, two times the initial average concentration. The reason is that the cross-sectional area of the connector is narrower than the pipe body; thus, the fluid velocity around the connector is faster. On the other hand, the drilling fluid and cuttings velocities are smaller behind the connector, so the cuttings are stacked as a pile.

4.2. Impact of the initial bed height

Fig. 9 presents contours of cuttings concentration under different initial bed heights. Observation shows that an increase in the initial bed height will cause a significant improvement in the cuttings concentration. Also, the impact of the initial bed height on average cuttings concentration is shown in Fig. 10. It can be demonstrated that with the initial height increases from 5% to 20% (the corresponding average cuttings concentration is from 1.2% to 9.3%), the highest average concentration rises from 3.6% to 16.0% (as high as 1.7–3.0 times the initial average concentration), which implies that the higher the cuttings bed, the harder it is to carry through the annulus; thus, it should wash the well to be clean enough before back reaming.

4.3. Impact of the diameter of the connector

Fig. 11 reveals the impact of varying the diameter of the connector with contours of cuttings concentration. The initial cuttings bed height is 10% d_o, and the packed porosity is 52%. Observation shows that after washing for 1 s, cuttings are accumulated behind the connector. An increase in the connector diameter results in a significant increase in the cuttings concentration behind the connector.

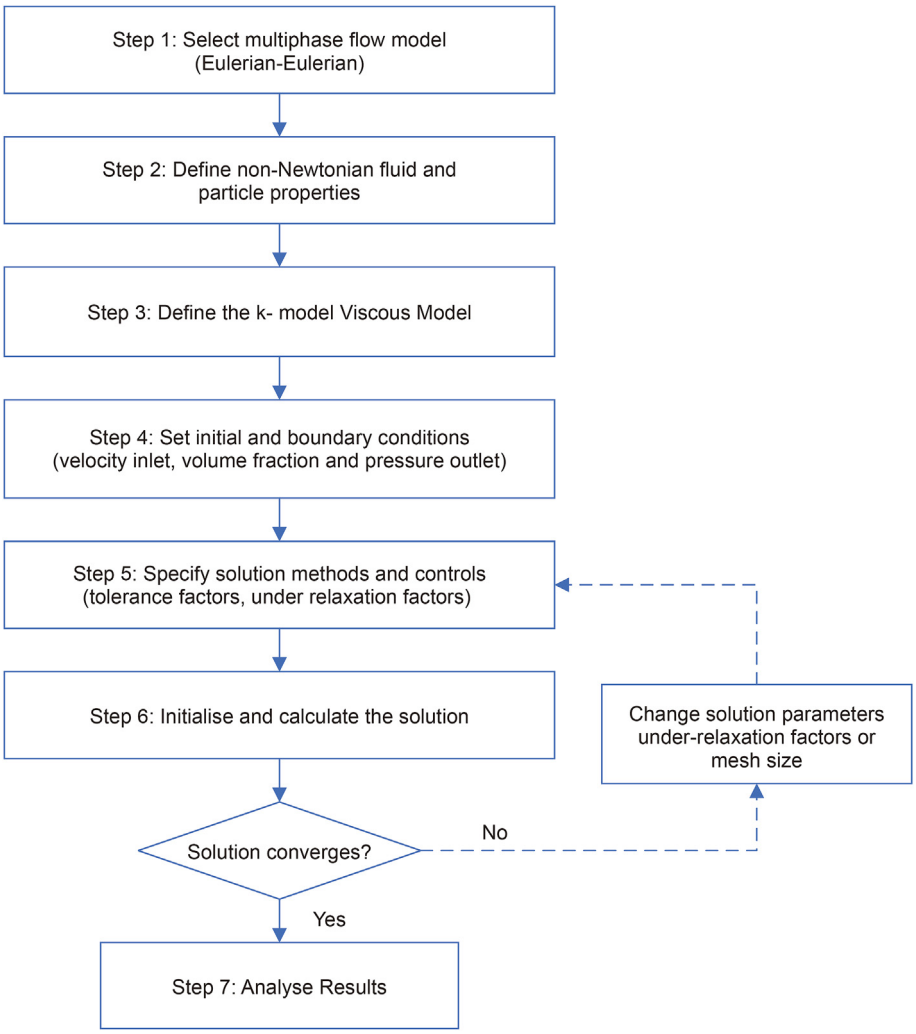

Fig. 5. Simulation procedure for the Eulerian–Granular model.

Also, it can be found that in Fig. 12, when the diameter of the connector increases from 42 to 54 mm, the maximum concentration at the interval of 1.2–1.5 m increases linearly from 6.5% to 10.5%, which is 1.1–1.7 times the initial average concentration. The piles behind the connector may make the pipe get stuck, especially when the diameter is more than 46 mm under the given eccentricity. This can serve as a guide for selecting the diameter of the connector.

4.4. Impact of the length of the connector

The length of the connector also affects the accumulated concentration. The contours of cuttings concentration under different connector lengths (0.250–0.625 m) and the average cuttings concentration of the cross-section along the horizontal pipe are depicted in Figs. 13 and 14. As can be manifested in Fig. 14, with the increase of the length of the connector from 0.250 to 0.625 m, the maximum cuttings concentration of the cross-section gradually decreases from 12.8% to 9.7%; however, the area with high cuttings concentration, for example, higher than 5%, become broader, which implies it would take longer to remove the cuttings below the connector with a more extended connector. This serves as an instruction for the cutting removal around the BHA, consisting of several tools and a longer length.

4.5. Impact of the inclination

In Fig. 15, contours of cuttings concentration under different inclinations are presented. The average cuttings concentration of the cross-section along the horizontal pipe and the maximum average concentration are illustrated in Figs. 16 and 17. Observation shows that when the inclination ascends from 20° to 90°, the cuttings concentration increases gradually from 3.6% to 12.8%. The cuttings concentration is most pronounced at the inclination of 60°, which is 12.9%. This is because the cuttings bed could slide down at certain flow conditions (known as the “avalanche” effect). Thus, more attention should be paid to the high-angle section while back reaming.

4.6. Impact of the rotation speed

The impact of the rotation speed of the drill pipe on the contours of the cuttings volume fraction is illustrated in Fig. 18. It can be observed that the cuttings concentration decreases with the pipe

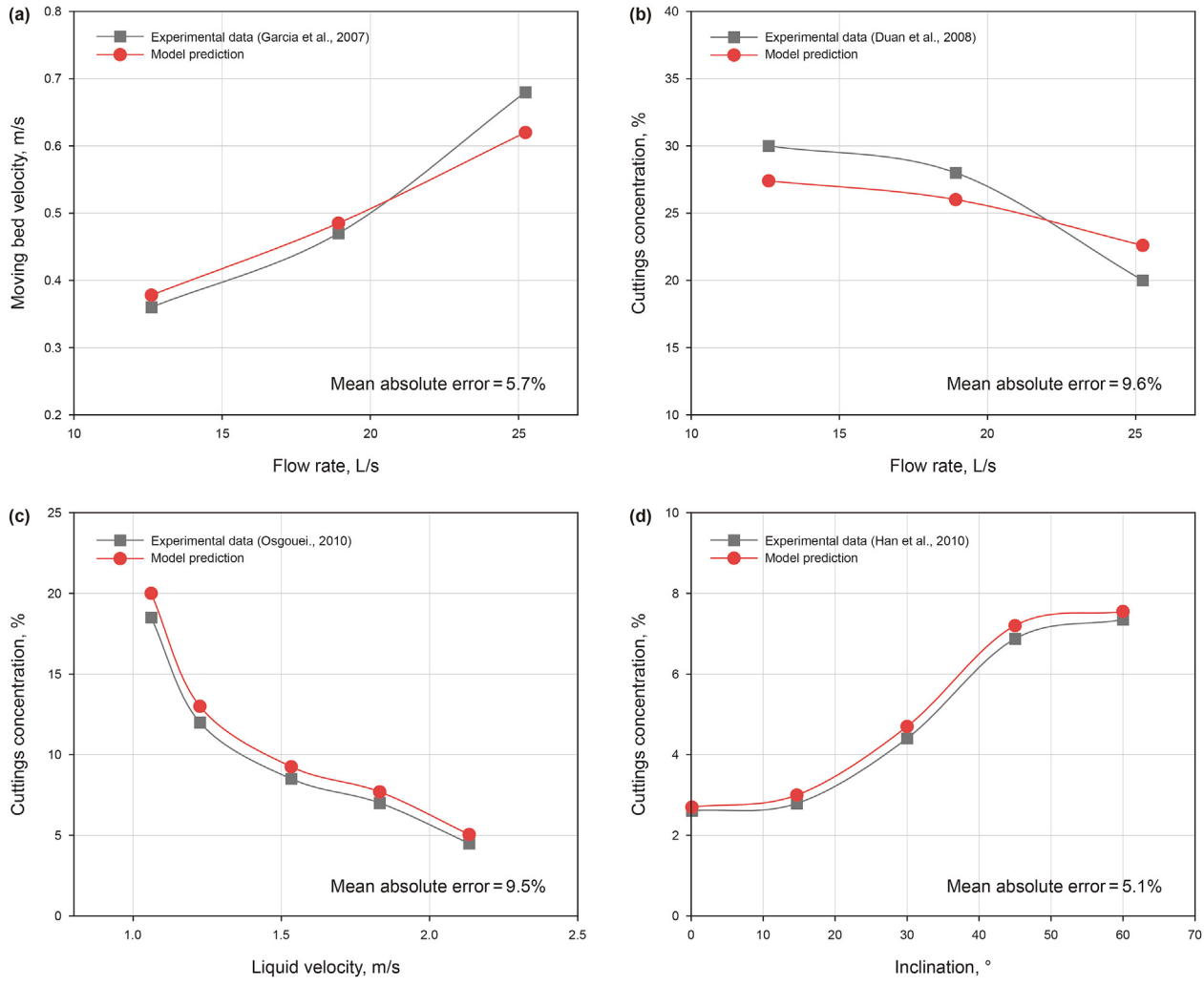

Fig. 6. Comparison of the CFD model simulation with the experiment data.

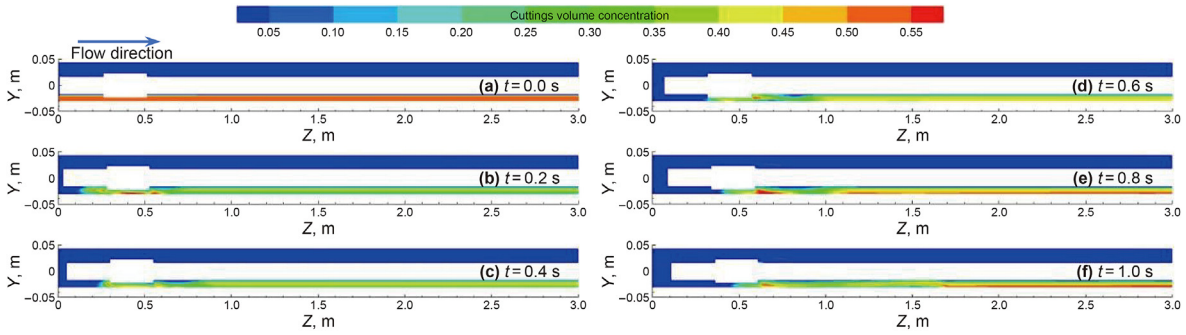

(a) Contours of cuttings volume concentration under different circulation time

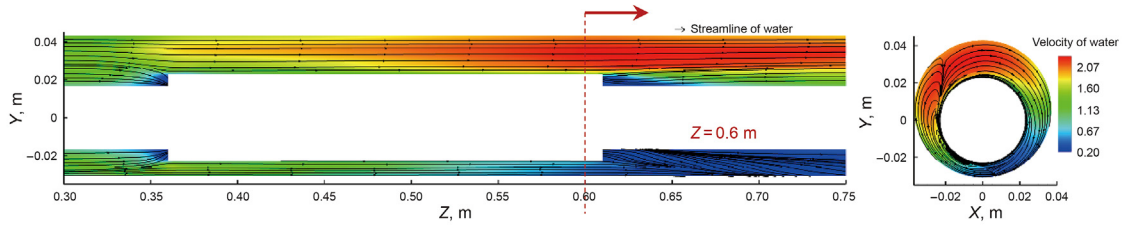

(b) Streamline distribution of water when $t = 1$ s

Fig. 7. Contours of cuttings volume concentration and the streamline of water.

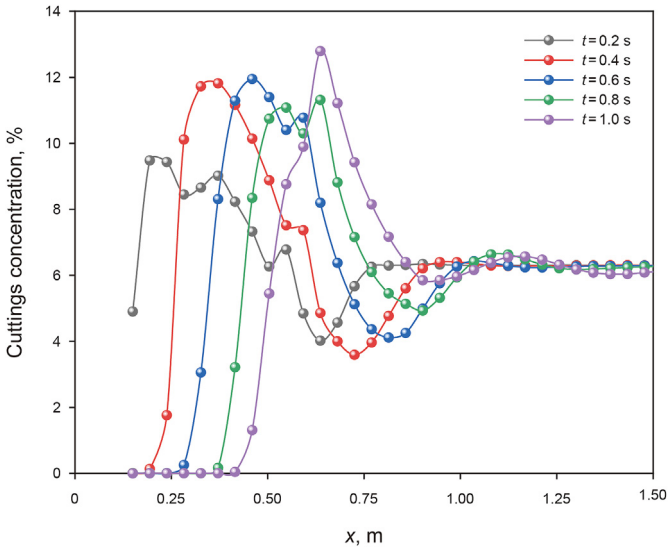

Fig. 8. The impact of the circulation time on average cuttings concentration.

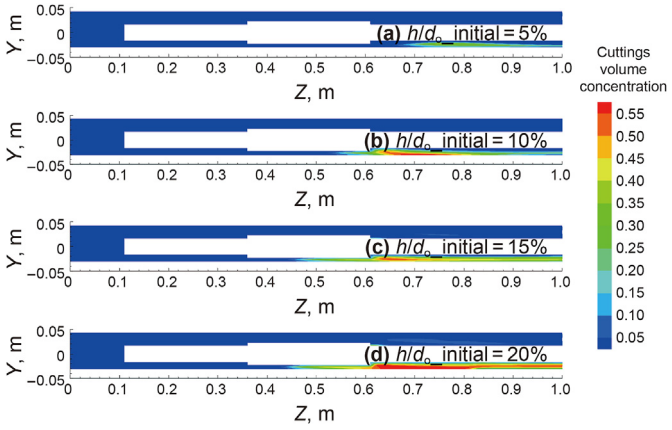

Fig. 9. Contours of cuttings volume concentration under different initial bed heights.

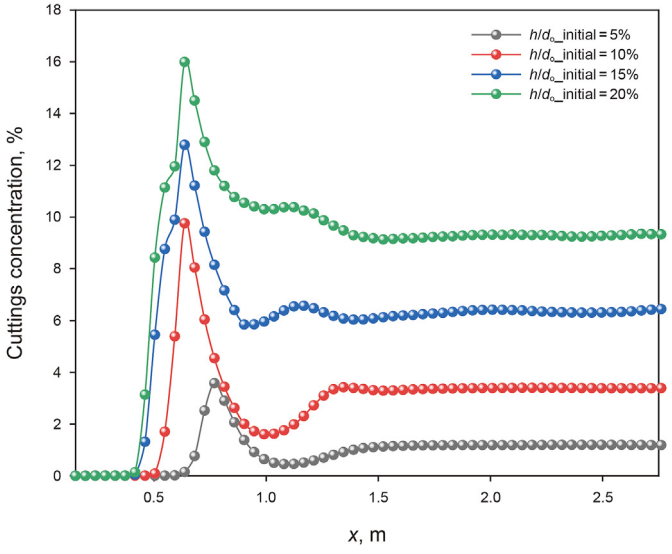

Fig. 10. The impact of the initial bed height on average cuttings concentration.

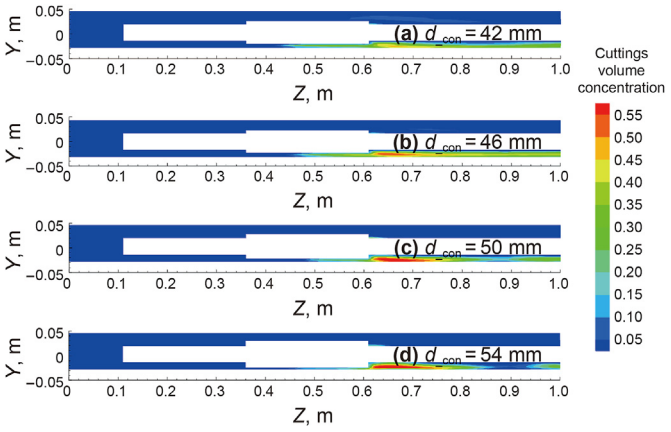

Fig. 11. Contours of cuttings volume concentration under different diameters of the connector.

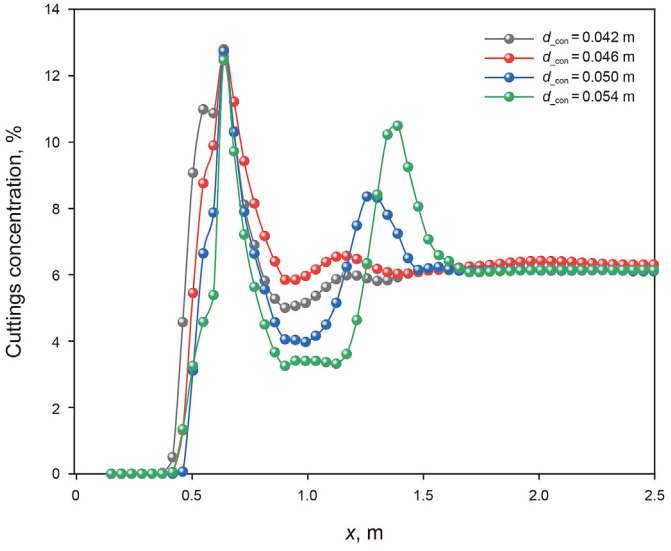

Fig. 12. The impact of the diameter of the connector on average cuttings concentration.

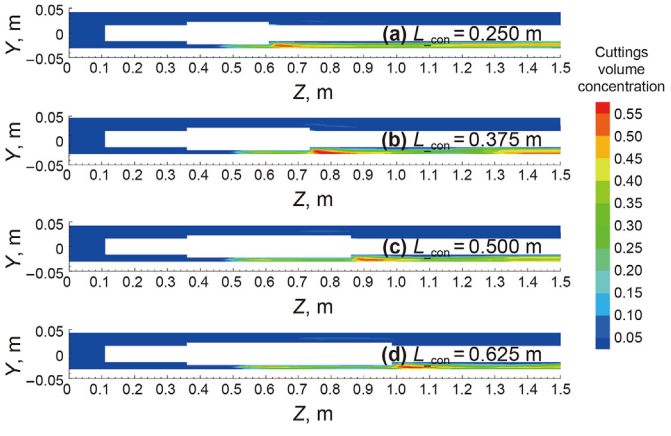

Fig. 13. Contours of cuttings volume concentration under different connector lengths.

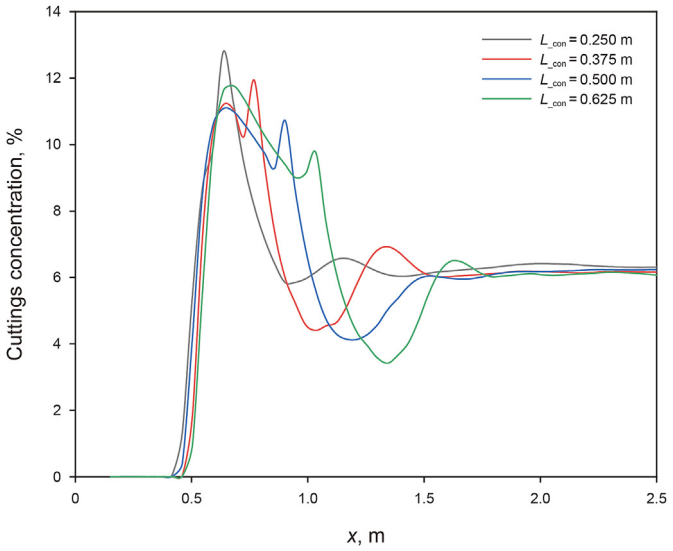

Fig. 14. The impact of the length of the connector on average cuttings concentration.

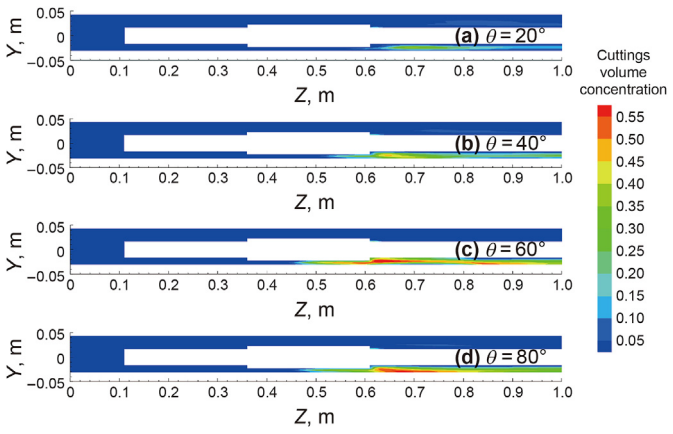

Fig. 15. Contours of cuttings volume concentration under different inclinations.

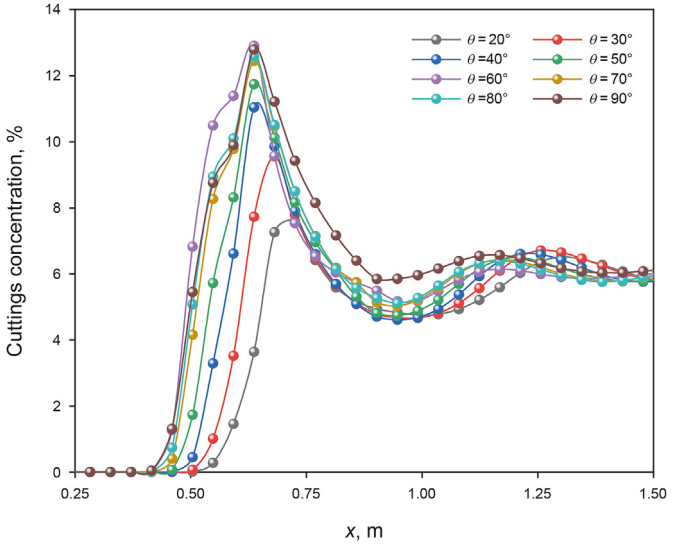

Fig. 16. The impact of the inclination on the average concentration of cuttings.

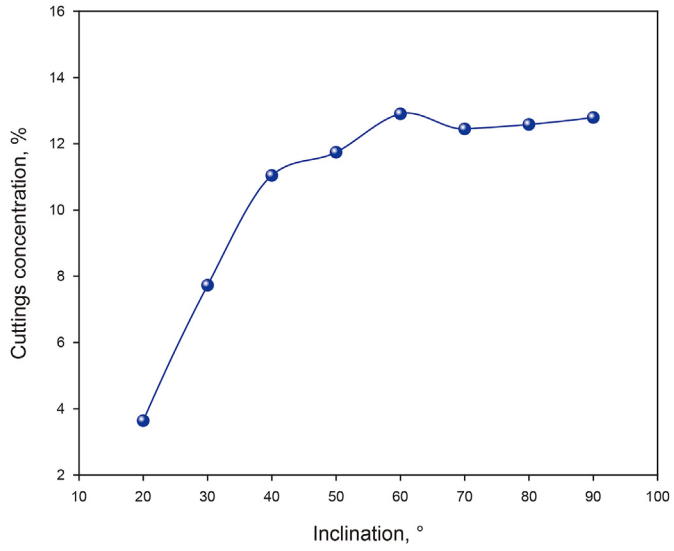

Fig. 17. The impact of the inclination on the maximum average cuttings concentration.

rotation speed significantly. Similarly, the cuttings are transported forward and pile up behind the connector. With the pipe rotation speed increasing from 0 to 180 RPM, the maximum cuttings concentration decreases from 13.5% to 11.0% (Fig. 19). This is because the pipe can disperse and lift the settled cuttings to the broader areas during rotation. Thus, increasing the pipe rotation speed benefits the cleaning efficiency significantly.

4.7. Impact of the consistency coefficient of the fluid

The effect of the power-law model (Li et al., 2016; Livescu, 2012) and different consistency coefficients have been investigated in Figs. 20 and 21. It can be observed that when transported by water, the maximum cuttings concentration is 12.8%. While transported by power-law drilling fluid, the maximum cuttings concentration decreases from 11.9% to 10.3% when the consistency coefficient increases from 0.5 to 0.9 Pa·s^n, which has better hole cleaning efficiency than water. The reason is that the power-law liquid has a higher viscosity and can provide greater shear force to transport the cuttings.

4.8. Impact of the flow behaviour index of the fluid

The effect of the power-law model and different flow behaviour indexes have been investigated in Figs. 22 and 23. It can be observed that when transported by water, the maximum cuttings concentration is 12.8%. While transported by power-law drilling fluid, the maximum cuttings concentration decreases from 11.9% to 10.1% when the flow behaviour index increases from 0.6 to 0.8, which has better hole cleaning efficiency than water. The reason is that the power-law liquid has a higher viscosity and can provide greater shear force to transport the cuttings.

4.9. Impact of the fluid density

The impact of the fluid density on contours and the average of cuttings volume fraction is illustrated in Figs. 24 and 25. It can be observed that with the fluid density increasing from 1000 to 1300 kg/m^3, the maximum cuttings concentration decreases from

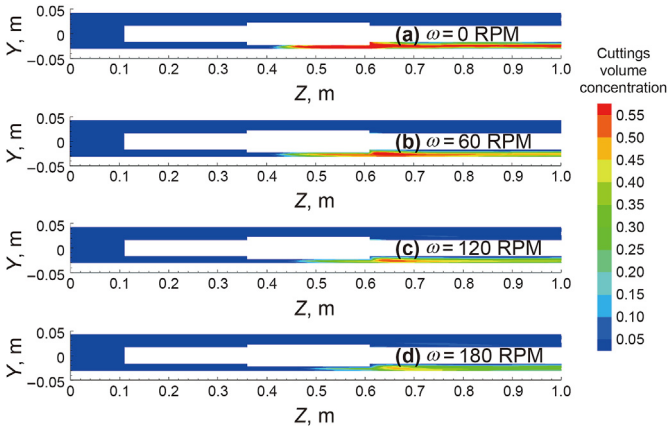

Fig. 18. Contours of cuttings volume concentration under different rotation speeds.

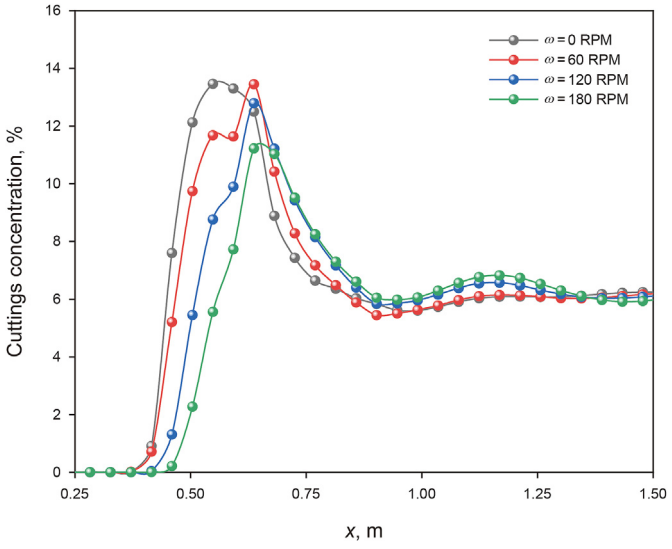

Fig. 19. The impact of the rotation speed on average cuttings concentration.

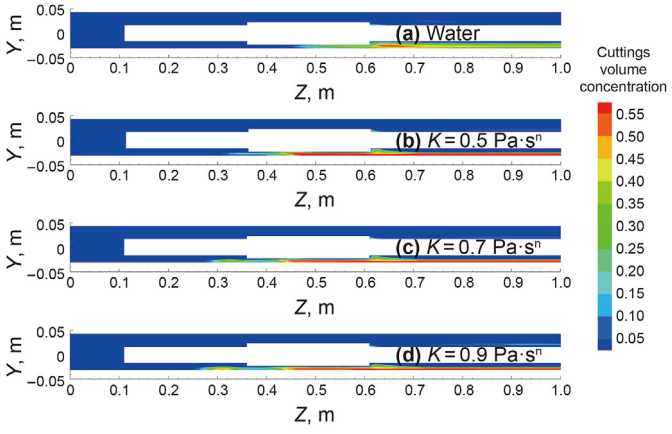

Fig. 20. Contours of cuttings volume concentration under different fluid consistency coefficients.

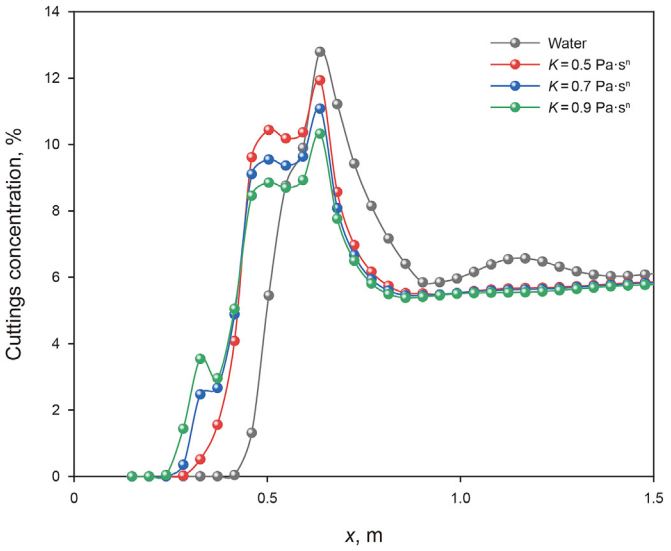

Fig. 21. The impact of the fluid consistency coefficient on average cuttings concentration.

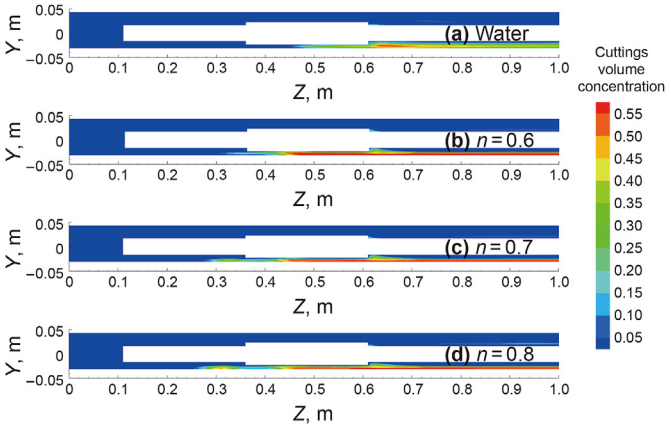

Fig. 22. Contours of cuttings volume concentration under different flow behaviour indexes.

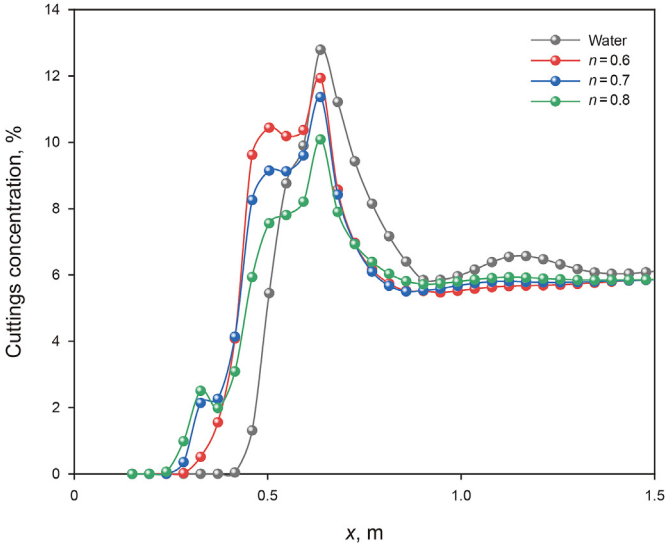

Fig. 23. The impact of the flow behaviour index on average cuttings concentration.

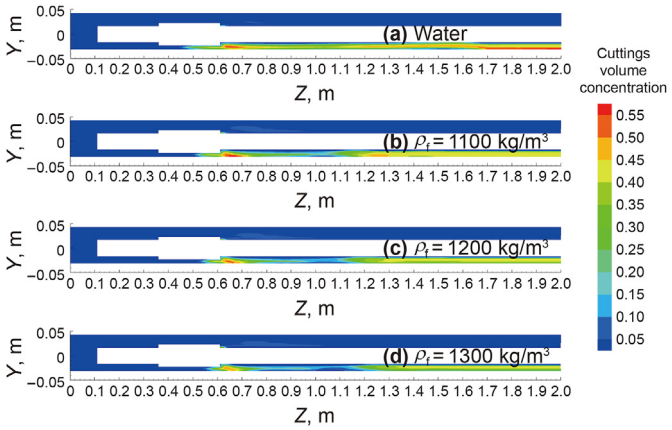

Fig. 24. Contours of cuttings volume concentration under different fluid densities.

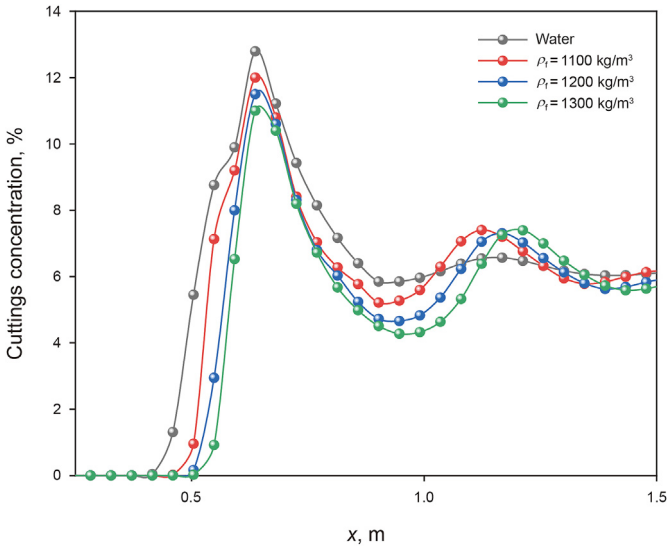

Fig. 25. The impact of the fluid density on average cuttings concentration.

12.7% to 11.1%, which indicates that the increase of the fluid density is beneficial to decreasing the cuttings concentration. This is because the higher the fluid density, the greater the buoyancy, and the easier it is for cuttings to be removed.

4.10. Impact of the tripping velocity

Fig. 26 depicts the contours of the cuttings volume concentration under the impact of different tripping velocities. The fluid inlet velocity is 0.75 m/s. It can be demonstrated in Fig. 26 that when tripping fast, there are cuttings remaining on the left side of the connector, which have not been removed. At the same time, cuttings also pile up on the right side of the connector. To figure out the sand concentration around the connector, Fig. 27 illustrates the impact of the tripping velocity on cuttings concentration based on four groups of fluid velocity (i.e., 0.25, 0.50, 0.75, 1.00 m/s).

As observed in Fig. 27, the tripping velocity significantly impacts the dune's appearance. On the one hand, when the pipe is tripping faster than the sand velocity (e.g., Fig. 27(a)), the sand piles up much higher behind the connector than that in front, and the average concentration distribution of the sand is in a convex shape. The reason is that the connector, like a "bulldozer", has a pushing effect on the sand when tripping fast.

On the other hand, when the tripping velocity is smaller than the sand velocity, for instance, when the tripping velocity is 0.2 m/s in Fig. 27(b), the sand is more likely to pile up at both ends of the connector in a concave shape. Because of the narrower cross-section area at the position of the connector than the pipe body, both the fluid and sand velocities become faster, which results in the accumulation at the two ends of the connectors.

It needs to be mentioned that the higher tripping velocity does not always lead to a higher dune. Take Fig. 27(a) for example; under the given fluid velocity, the maximum cuttings concentrations under different tripping velocities are almost the same after simulation for 1 s. The most crucial factor is the relationship between tripping velocity and cuttings' velocity. As depicted in Fig. 27(c), the accumulated dune with the convex shape is higher than the concave one under the given fluid velocity, which means the "bulldozer" effect of the connector exercises a more severe impact on hole cleaning. So, the tripping velocity is suggested to be slower than the sand while back reaming.

4.11. Impact of the fluid inlet velocity

Fig. 28 depicts the contours of the cuttings volume concentration under different fluid inlet velocities when the tripping velocity is 0.2 m/s, and Fig. 29 shows the impact of the fluid inlet velocity on the cuttings concentration based on four different groups of tripping velocity (i.e., 0.2, 0.4, 0.6, 0.8 m/s).

As observed in Fig. 28, the cuttings bed moves faster with a higher fluid inlet velocity. However, we cannot simply conclude that the higher fluid velocity is more beneficial to the hole cleaning while back reaming. It is because a higher fluid velocity may also

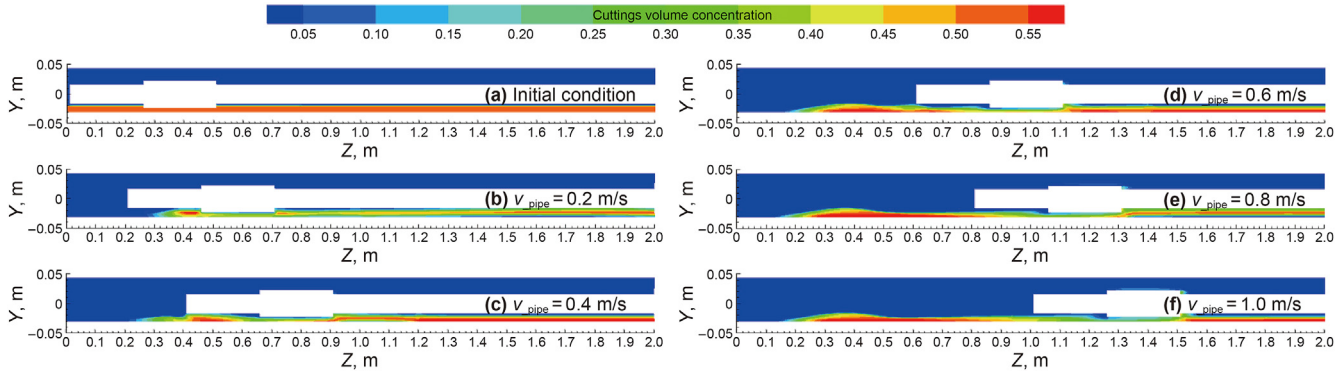

Fig. 26. Contours of cuttings volume concentration under different tripping velocities. (fluid inlet velocity is 0.75 m/s).

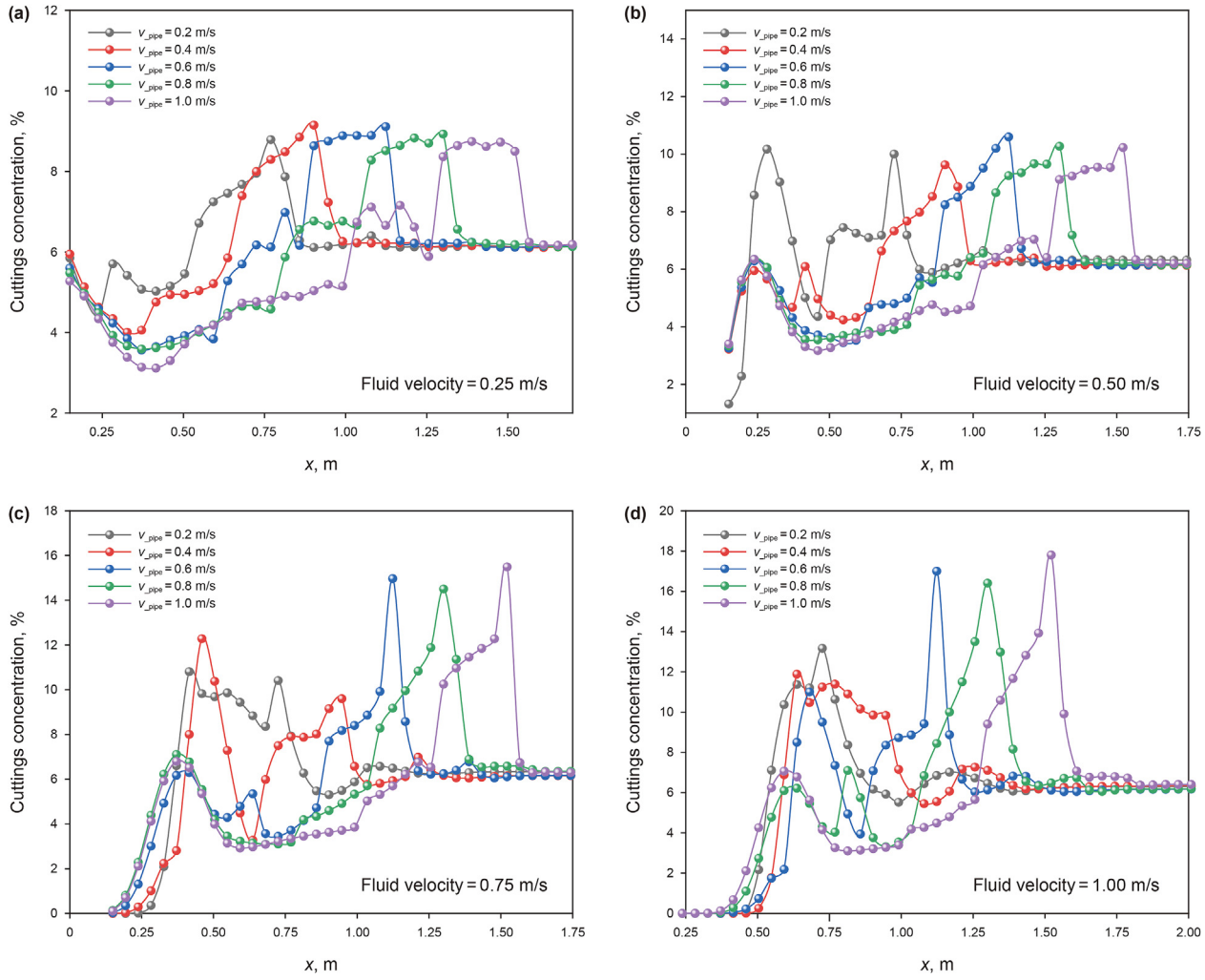

Fig. 27. The impact of the tripping velocity on average cuttings concentration (fluid inlet velocities are 0.25, 0.50, 0.75, 1.00 m/s).

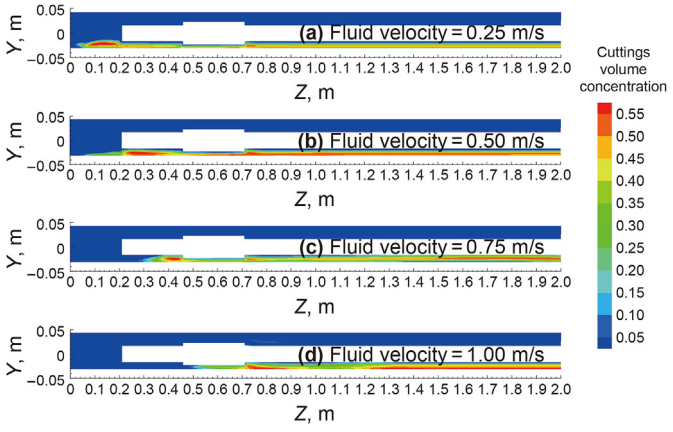

Fig. 28. Contours of cuttings volume concentration under different fluid velocities. (tripping velocity is 0.2 m/s).

lead to a higher accumulation of sand around the connector, which may lead to the pipe getting stuck. For instance, the tripping velocity is 0.6 m/s, and when the fluid inlet velocity rises from 0.25 to 0.75 m/s, the accumulated cuttings concentration rises from 6.7% to 14.9% (Fig. 29(c)). The reason is that the cuttings bed has not completely passed through the connector, and a higher fluid inlet velocity may transport more cuttings to pile up behind the connector. So, to take advantage of the significant flow rate, it is safer to wait until the cuttings are transported behind the connector, such as the BHA.

5. Conclusions

(1) A coupled layering-sliding mesh method with a Eulerian-Granular approach is proposed innovatively to investigate the cuttings transport while back reaming. The dynamic layering method is employed to simulate the axial movement of the pipe, whereas the sliding mesh model simulates the pipe rotation. Both translation and rotation of the pipe have been successfully simulated.

(2) The increase in the inclination, the initial bed height, the diameter, and the length of the connector will cause a significant increase in the cuttings concentration. The cuttings concentration decreases with the pipe rotation speed significantly.

(3) Moreover, the higher tripping velocity does not always lead to a higher dune, and there are two main factors contribute towards the cuttings accumulation around the connector,

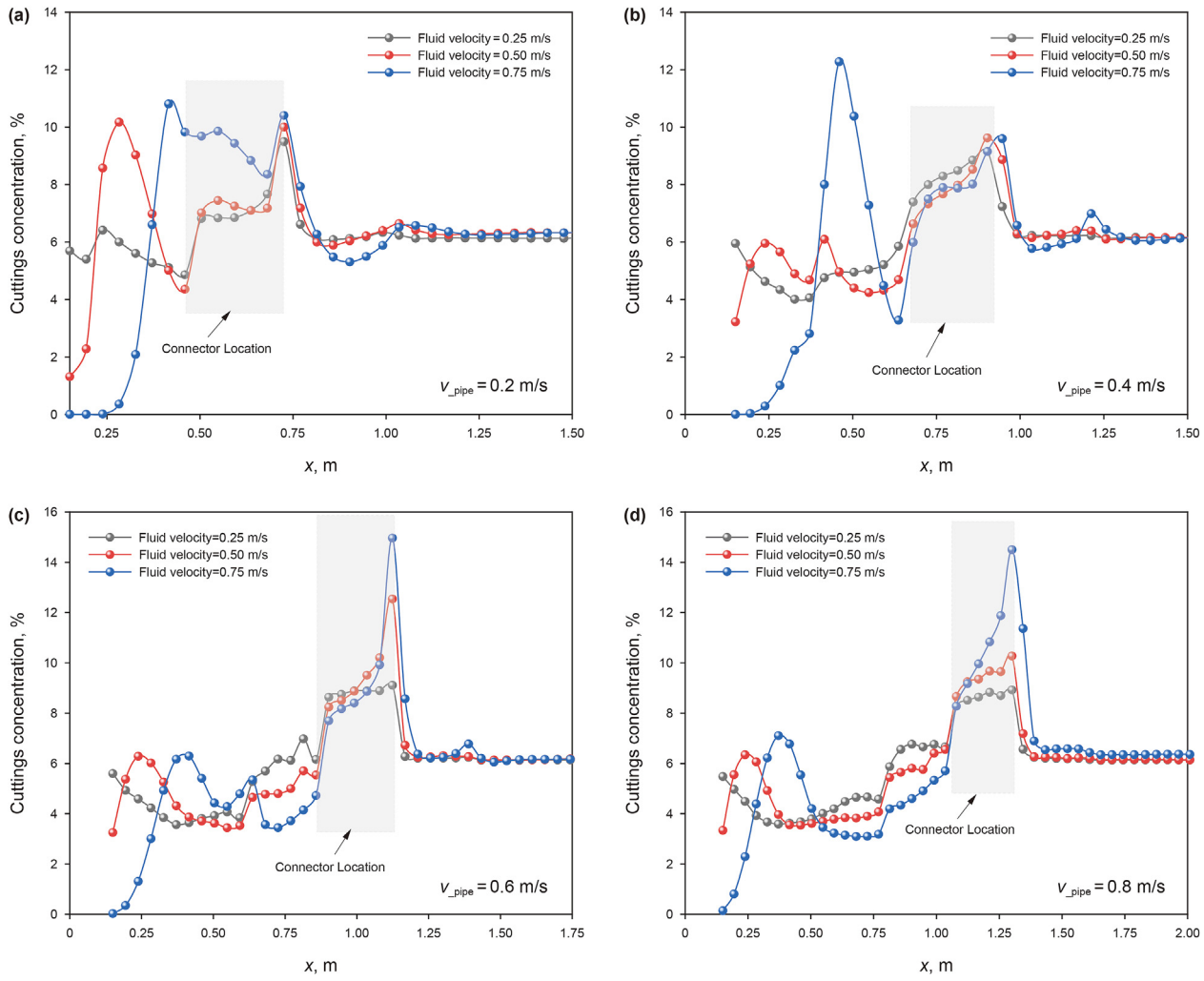

Fig. 29. The impact of the fluid velocity on average cuttings concentration (tripping velocities are 0.2, 0.4, 0.6, 0.8 m/s).

namely, the difference in the cross-sectional area and the pushing effect of the connector, like a "bulldozer". When the tripping velocity is larger than the cuttings, the connector's "bulldozer" effect dominates. Conversely, the effect of the cross-sectional area difference is the leading factor for cuttings accumulation. The "bulldozer" effect of the connector exercises a more severe impact on hole cleaning. The accumulated bed height under different tripping velocities in both cases varies mildly. Thus, the tripping velocity is suggested to be slower than the sand during the back reaming operation.

(4) Furthermore, considering the existence of a connector, the inlet velocity might turn from a positive to a negative factor for hole cleaning. An increase in the fluid velocity may lead to a higher accumulated cuttings concentration around the connector when the cuttings bed has not completely passed through the connector. A significant flow rate can be safely applied after the cuttings have passed through the connector furnished with a large diameter, such as the BHA.

(5) The limitation of the current model is that the effect of the particle shape and the detailed structure of the connector is not considered. Complex structure of the connector, such as the cuttings bed remover, can be analyzed further to investigate the effect of the tools on cuttings transport. Moreover, the particle trajectory can be investigated further via CFD-DEM model. However, the CFD-DEM model with the dynamic mesh method may need much more computing resources.

Declaration of competing Interest

The authors declare that they have no known competing financial interests or personal relationships that could have appeared to influence the work reported in this paper.

Acknowledgements

The authors gratefully acknowledge the financial support from the Natural Science Foundation of China (Grant Nos. 52222401, 52234002, 51904317 and 52174012), Science Foundation of China University of Petroleum, Beijing (Grant No. ZXZX20230083), and other projects (ZLZX2020-01-07-01).

Appendix A. Table of the comparison of Eulerian-Eulerian and Eulerian-Lagrangian methods for the solid-liquid two-phase flow

Table 1a
The comparison of Eulerian-Eulerian and Eulerian-Lagrangian methods for the solid-liquid two-phase flow.

	Model	Numerical approach	Particle-Particle interaction	Advantage	Disadvantage
Eulerian-Eulerian	Eulerian-Granular	Fluid- Eulerian Particles- Eulerian	P–P interactions are modeled by fluid properties, such as granular pressure, viscosity, drag, etc.	Faster calculation speed and less computational cost.	Unable to track the motion of each particle separately and consider the particle collisions.
Eulerian-Lagrangian	DPM	Fluid-Eulerian Particles -Lagrangian	Neglected	More computational cost and slower calculation speed.	Able to track the motion of each particle separately and consider the particle collisions.
	DDPM-KTGH	Fluid-Eulerian Particles -Lagrangian	Approximate interactions determined by granular models.		
	DDPM-DEM	Fluid- Eulerian Particles- Eulerian	Accurate determination of P–P interactions.		

References

Akhshik, S., Behzad, M., Rajabi, M., 2015. CFD-DEM approach to investigate the effect of drill pipe rotation on cuttings transport behavior. J. Pet. Sci. Eng. 127, 229–244. https://doi.org/10.1016/j.petrol.2015.01.017.

Alshaikh, A.A., Albassam, M.K., Al Gharbi, S.H., et al., 2018, 12-15 November. In: Detection of Stuck Pipe Early Signs and the Way toward Automation. UAE, Abu Dhabi. https://doi.org/10.2118/192975-MS.

Basu, D., Das, K., Smart, K., et al., 2015. Comparison of eulerian-granular and discrete element models for simulation of proppant flows in fractured reservoirs, 13-19 November. In: Abu Dhabi International Petroleum Exhibition & Conference. Houston, Texas. https://doi.org/10.1115/IMECE2015-50050.

Bicalho, I.C., Dos Santos, D.B.L., Ataíde, C.H., et al., 2016. Fluid-dynamic behavior of flow in partially obstructed concentric and eccentric annuli with orbital motion. J. Pet. Sci. Eng., ASME International Mechanical Engineering Congress and Exposition 137, 202–213. https://doi.org/10.1016/j.petrol.2015.11.029.

Bonamy, D., Chavanis, P.H., Cortet, P.P., et al., 2009. Euler-like modelling of dense granular flows: application to a rotating drum. Eur. Phys. J. B. 68, 619–627. https://doi.org/10.1140/epjb/e2009-00123-6.

Capecelatro, J., Desjardins, O., 2013. An Euler-Lagrange strategy for simulating particle-laden flows. J. Comput. Phys. 238, 1–13. https://doi.org/10.1016/j.jcp.2012.12.015.

Cayeux, E., Mesagan, T., Tanripada, S., et al., 2014. Real-time evaluation of hole-cleaning conditions with a transient cuttings-transport model. SPE Drill. Complet. 29 (1), 5–21. https://doi.org/10.2118/163492-PA.

Cho, H., Shan, S.N., Osisanya, S.O., 2002. A three-segment hydraulic model for cuttings transport in coiled tubing horizontal and deviated drilling. J. Can. Pet. Technol. 42, 32–39. https://doi.org/10.2118/02-06-03.

Duan, M., Miska, S., Yu, M., et al., 2008. Transport of small cuttings in extended-reach drilling. SPE Drill. Complet. 23 (3), 258–265. https://doi.org/10.2118/104192-PA.

Epelle, E.I., Gerogiorgis, D.I., 2019. Drill cuttings transport and deposition in complex annular geometries of deviated oil and gas wells: a multiphase flow analysis of positional variability. Chem. Eng. Res. Des. 151, 214–230. https://doi.org/10.1016/j.cherd.2019.09.013.

Fluent, A., 2021. ANSYS Fluent Theory Guide 2021 R2.

Garcia-Hernandez, A.J., Miska, S.Z., Yu, M., et al., 2007. Determination of cuttings lag in horizontal and deviated wells, 11-14 November. In: SPE Annual Technical Conference and Exhibition. Anaheim, California, USA. https://doi.org/10.2118/109630-MS.

Gavignet, A., Sobey, I., 1989. Model aids cuttings transport prediction. J. Petrol. Technol. 41 (9), 916–921. https://doi.org/10.2118/15417-PA.

Guo, X.-l., Wang, Z.-m., Long, Z.-h., 2010. Study on three-layer unsteady model of cuttings transport for extended-reach well. J. Petrol. Sci. Eng. 73 (1–2), 171–180. https://doi.org/10.1016/j.petrol.2010.05.020.

Han, S., Hwang, Y., Woo, N., Kim, Y., 2010. Solid–liquid hydrodynamics in a slim hole drilling annulus. J. Pet. Sci. Eng. 70 (3–4), 308–319. https://doi.org/10.1016/j.petrol.2009.12.002.

Heydari, O., Sahraei, E., Skalle, P., 2017. Investigating the impact of drillpipe's rotation and eccentricity on cuttings transport phenomenon in various horizontal annuluses using computational fluid dynamics (CFD). J. Pet. Sci. Eng. 156, 801–813. https://doi.org/10.1016/j.petrol.2017.06.059.

Li, J., Luft, B., 2014a. Overview of solids transport studies and applications in oil and gas industry-experimental work, 14-16 October. In: SPE Russian Oil and Gas Exploration & Production Technical Conference and Exhibition. Moscow, Russia. https://doi.org/10.2118/171285-MS.

Li, J., Luft, B., 2014b. Overview solids transport study and application in oil-gas industry-theoretical work, 10-12 December. In: International Petroleum Technology Conference. Kuala Lumpur, Malaysia. https://doi.org/10.2523/IPTC-17832-MS.

Li, W., Zhao, X., Ji, Y., Peng, H., et al., 2016. Investigation of biodiesel-based drilling fluid, Part 2: formulation design, rheological study, and laboratory evaluation. SPE J. 21 (5), 1767–1781.

Livescu, S., 2012. Mathematical modeling of thixotropic drilling mud and crude oil flow in wells and pipelines—a review. J. Petrol. Sci. Eng. 98, 174–184.

Mahmoud, H., Ahmed, H., Nasser, M.S., et al., 2020. Hole cleaning and drilling fluid sweeps in horizontal and deviated wells: comprehensive review. J. Pet. Sci. Eng. 186, 1–15. https://doi.org/10.1016/j.petrol.2019.106748.

Nguyen, D., Rahman, S.S., 1998. A three-layer hydraulic program for effective cuttings transport and hole cleaning in highly deviated and horizontal wells. SPE Drill. Complet. 13 (3), 182–189. https://doi.org/10.2118/51186-PA.

Osgouei, E., 2010. Determination of Cuttings Transport Properties of Gasified Drilling Fluids. Middle East Technical University. Doctoral thesis.

Ozbayoglu, M.E., Saasen, A., Sorgun, M., et al., 2008. Effect of pipe rotation on hole cleaning for water-based drilling fluids in horizontal and deviated wells. In: IADC/SPE Asia Pacific Drilling Technology Conference and Exhibition. 25-27 August, Jakarta, Indonesia. https://doi.org/10.2118/114965-MS.

Pandya, S., Ahmed, R., Shah, S., 2019. Effects of particle density on hole cleanout operation in horizontal and inclined wellbores. In: SPE/ICoTA Well Intervention Conference and Exhibition. 26-27 March, The Woodlands, Texas, USA. https://doi.org/10.2118/194240-MS.

Pang, B., Wang, S., Lu, C., Cai, W., Jiang, X., Lu, H., 2019. Investigation of cuttings transport in directional and horizontal drilling wellbores injected with pulsed drilling fluid using CFD approach. Tunn. Undergr. Space Technol. 90, 183–193. https://doi.org/10.1016/j.tust.2019.05.001.

Paranhos Sobrinho, E.S., Escarpini Filho, R.S., Lages, E.N., et al., 2021. Consideration of backreaming in vertical wells closure modeling in salt rock. SPE J. 26 (3), 1092–1109. https://doi.org/10.2118/204209-PA.

Ramírez, L., Foulquié, C., Nogueira, X., et al., 2015. New high-resolution-preserving sliding mesh techniques for higher-order finite volume schemes. Comput. Fluids 118, 114–130. https://doi.org/10.1016/j.compfluid.2015.06.008.

Song, X., Xu, Z., Wang, M., et al., 2017. Experimental study on the wellbore-cleaning efficiency of microhole-horizontal-well drilling. SPE J. 22 (4), 1189–1200. https://doi.org/10.2118/185965-PA.

Yarim, G., Ritchie, G.M., May, R.B.J.S.D., 2010. A guide to successful backreaming: real-time case histories. SPE Drill. Complet. 25 (1), 27–38. https://doi.org/10.2118/116555-PA.

Yarim, G., Uchytil, R.J., May, R.B., et al., 2007. Stuck pipe prevention—a proactive solution to an old problem, 11-14 November, 2007. In: SPE Annual Technical Conference and Exhibition. U.S.A, California. https://doi.org/10.2118/109914-MS.

Zhang, B., Liang, C.J.J.o., 2015. A simple, efficient, and high-order accurate curved sliding-mesh interface approach to spectral difference method on coupled rotating and stationary domains. J. Comput. Phys. 295, 147–160. https://doi.org/10.1016/j.jcp.2015.04.006.

Zhang, F., Miska, S., Yu, M., et al., 2018. A unified transient solid-liquid two-phase flow model for cuttings transport-modelling part. J. Pet. Sci. Eng. 166, 146–156. https://doi.org/10.1016/j.petrol.2018.03.027.

Zhang, F., Wang, Y., Wang, Y., et al., 2020. Modeling of dynamic cuttings transportation during drilling of oil and gas wells by combining 2D CFD and 1D discretization approach. SPE J. 25 (3), 1220–1240. https://doi.org/10.2118/199902-PA.

Zhu, N., Huang, W., Gao, D., 2022. Numerical analysis of the stuck pipe mechanism related to the cutting bed under various drilling operations. J. Pet. Sci. Eng. 208, 109783. https://doi.org/10.1016/j.petrol.2021.109783.